



University of
Massachusetts
Amherst

Feedback And Recycled Wind Accretion: Assembling The $Z = 0$ Galaxy Mass Function

Item Type	Article
Authors	Oppenheimer, BD;Dave, R;Keres, D;Fardal, M;Katz, N;Kollmeier, JA;Weinberg, D
DOI	10.1111/j.1365-2966.2010.16872.x
Download date	2026-04-20 00:18:01
Link to Item	https://hdl.handle.net/20.500.14394/3568

Feedback and Recycled Wind Accretion: Assembling the $z = 0$ Galaxy Mass Function

Benjamin D. Oppenheimer^{1,2}, Romeel Davé², Dušan Keresš³, Mark Fardal⁴, Neal Katz⁴, Juna A. Kollmeier⁵, David H. Weinberg^{6,7}

¹ *Leiden Observatory, Leiden University, PO Box 9513, 2300 RA Leiden, the Netherlands*

² *Astronomy Department, University of Arizona, Tucson, AZ 85721, USA*

³ *Harvard-Smithsonian Center for Astrophysics, Cambridge, MA 02138, USA*

⁴ *Astronomy Department, University of Massachusetts, Amherst, MA 01003, USA*

⁵ *Observatories of the Carnegie Institution of Washington, Pasadena, CA 91101, USA*

⁶ *Astronomy Department, Ohio State University, Columbus, OH 43210, USA*

⁷ *Institute for Advanced Study, Princeton, NJ 08450, USA*

14 May 2010

ABSTRACT

We analyse cosmological hydrodynamic simulations that include theoretically and observationally motivated prescriptions for galactic outflows. If these simulated winds accurately represent winds in the real Universe, then material previously ejected in winds provides the dominant source of gas infall for new star formation at redshifts $z < 1$. This recycled wind accretion, or *wind mode*, provides a third physically distinct accretion channel in addition to the “hot” and “cold” modes emphasised in recent theoretical studies. The recycling time of wind material (t_{rec}) is shorter in higher-mass systems owing to the interaction between outflows and the increasingly higher gas densities in and around higher-mass halos. This *differential recycling* plays a central role in shaping the present-day galaxy stellar mass function (GSMF), because declining t_{rec} leads to increasing wind mode galaxy growth in more massive halos. For the three feedback models explored, wind mode dominates above a threshold mass that primarily depends on wind velocity; the shape of the GSMF therefore can be directly traced back to the feedback prescription used. If we remove all particles that were ever ejected in a wind, then the predicted GSMFs are much steeper than observed. In this case galaxy masses are suppressed both by the ejection of gas from galaxies and by the hydrodynamic heating of their surroundings, which reduces subsequent infall. With wind recycling included, the simulation that incorporates our favoured momentum-driven wind scalings reproduces the observed GSMF for stellar masses $10^9 M_{\odot} \leq M \leq 5 \times 10^{10} M_{\odot}$. At higher masses, wind recycling leads to excessive galaxy masses and star formation rates relative to observations. In these massive systems, some quenching mechanism must suppress not only the direct accretion from the primordial IGM but the re-accretion of gas ejected from star-forming galaxies. In short, as has long been anticipated, the form of the GSMF is governed by outflows; the unexpected twist here for our simulated winds is that it is not primarily the ejection of material but how the ejected material is re-accreted that governs the GSMF.

Key words: galaxies: formation, assembly, low redshift; intergalactic medium; cosmology: theory; methods: numerical

1 INTRODUCTION

A fundamental challenge in galaxy formation theory is to understand the mechanisms that shape the observed galaxy stellar mass function (GSMF). This requires understanding how galaxies form and grow within dark matter halos. Observations and theory indicate that the relation of galactic stellar components to underlying dark matter halos is not

simple. In the mass range corresponding to halos of individual galaxies, the dark matter halo mass function, $\Phi(M_h)$, follows roughly $dn/dM_h \sim M_h^{-2}$ (e.g. Sheth & Tormen 1999; Jenkins et al. 2001; Springel et al. 2005), turning over only in the group mass range. On the other hand, the GSMF, $\Phi(M_s)$, is most often fit using a Schechter function, $dn/dM_s \sim M_s^{\alpha} \exp(-M_s/M^*)$ (Schechter 1976), where M_s

is stellar mass and $z = 0$ M^* is roughly the mass of the Milky Way. The low-mass slope α is much shallower than -2 (e.g. Baldry et al. 2008). Hence the efficiency of star formation decreases at masses both lower and higher than M^* . *A theory of galaxy formation must explain the following features of the GSMF: a preferred mass for star formation efficiency, a shallow low-mass end slope, and a rapid drop at large masses.*

We categorise physical mechanisms that imprint features on the GSMF into two classes: those having to do with how galaxies obtain baryons (“accretion”), and those having to do with how galaxies lose baryons (“feedback”). For accretion, the cooling of the hot virialised atmospheres, i.e. “hot mode” accretion, was historically believed to be the main channel of gas supply to galaxies. Models of this process give a characteristic mass above which gas in a gravitationally contracting halo cannot cool in a Hubble time (t_H) to form stars (Rees & Ostriker 1977; Silk 1977; White & Rees 1978), thereby providing a turnover in the theoretical GSMF, though in the absence of feedback the implied mass scale is higher and the cutoff shallower than observed (White & Frenk 1991; Thoul & Weinberg 1995; Benson et al. 2003).

More recently, “cold mode” accretion was argued to be responsible for most of the gas supply into galaxies across cosmic time (Katz et al. 2003; Kereš et al. 2005, hereafter K05; Dekel & Birnboim 2006). In cold mode, gas is supplied via cold filaments that rapidly stream gas from the intergalactic medium (IGM) into star-forming regions, without ever encountering a virial shock (Binney 1977; Birnboim & Dekel 2003). This is most effective in lower-mass halos, while in halos $\gtrsim 10^{12} M_\odot$ shocked gas dominates the halo gas, although dense filaments at high redshifts ($z \gtrsim 2$) still allow cold mode accretion to proceed even above this threshold mass (K05; Dekel & Birnboim 2006; Kereš 2007; Ocvirk et al. 2008; Kereš et al. 2009a, hereafter K09a; Brooks et al. 2009; Dekel et al. 2009). At lower redshifts, the supply of cold gas declines in massive halos, and the cooling of the hot atmosphere becomes relatively more important (K09a). This late hot mode is relatively inefficient and can be naturally prevented in the large, constant density cores of cluster halos.

Yet accretion alone cannot be the entire story, as it is well known that without strong feedback, models fail to produce basic observations such as the luminosity function and the GSMF (Kauffmann et al. 1993; Cole et al. 1994; Murali et al. 2002; Bower et al. 2006). Kereš et al. (2009b, hereafter K09b) explored a cosmological SPH simulation without any form of explicit feedback and derived a “correction factor” as a function of stellar mass to correct the simulated GSMF to match the observed one. The fact that their correction factor is always greater than one exemplifies the “over-cooling” problem in galaxy formation, where the efficiency of forming stars, based on simple theoretical expectations, is greater than that actually observed (e.g. White & Frenk 1991; Balogh et al. 2001). *Distinct feedback processes may operate at different mass scales*, given that star formation needs to be suppressed by ~ 10 at $M_s < 10^{10} M_\odot$, falling to only ~ 2 at $10^{11} M_\odot$, and then increasing again to ~ 5 by $10^{12} M_\odot$ (see f_{corr} plotted in K09b, Figure 1).

K09b differentiated “preventive” feedback, where a pro-

cess prevents gas from entering a galaxy’s ISM in the first place, and “ejective” feedback, where gas is accreted and then thrown back out. Preventive feedback is most applicable for hot mode, since halos with dilute hot atmospheres can be more effectively kept hot by feedback processes such as jets from active galactic nuclei (AGN) and magnetic conduction (e.g. Binney 2004, K05). An example of preventive feedback affecting hot mode is “radio”-mode feedback (Best et al. 2005; Croton et al. 2006). However, K09b showed that preventing hot mode accretion alone is insufficient to correct the GSMF, since in large systems most of the stars are still formed via cold mode when the galaxy was smaller (K09a), meaning that *cold mode must be suppressed*. Preventing cold mode accretion is much more challenging, since this gas is streaming in via dense filaments that are not easily disrupted. Hence, even for galaxies that are today dominated by hot mode accretion, ejective feedback appears necessary to understand their present-day stellar masses.

In short, both the high and low ends of the observed GSMF appear to *require an ejective feedback mechanism* to curtail cold mode-driven star formation. A leading candidate for such a mechanism is galactic winds (e.g. Dekel & Silk 1986). Winds ejecting galactic ISM have the added benefit of chemically enriching the IGM, where metal absorption lines are observed to be common (e.g. Songaila & Cowie 1996; Songaila 2001; Schaye et al. 2003; Simcoe et al. 2004; Adelberger et al. 2005). Star formation suppression, IGM enrichment, plus the ubiquity of escaping outflows observed in star forming galaxy spectra (e.g., Pettini et al. 2001; Shapley et al. 2003; Martin 2005a; Weiner et al. 2009) have motivated the inclusion of star formation based feedback prescriptions in cosmological simulations (Springel & Hernquist 2003b; Kobayashi 2004; Cen & Ostriker 2006; Oppenheimer & Davé 2006; Sommer-Larson & Fynbo 2008; Wiersma et al. 2009b). Oppenheimer & Davé (2006) explored a range of feedback prescriptions, finding that the scalings predicted by a momentum-driven wind model (Murray, Quatert, & Thompson 2005) were most promising for matching the observations of high- z IGM enrichment. In this scenario, wind velocity (v_{wind}) scales with galaxy velocity dispersion (σ), leading to the gradual enrichment of the IGM matching the observed frequency of $z \sim 6$ C IV lines (Oppenheimer, Davé, & Finlator 2009), the evolution of C IV from $z = 5 \rightarrow 2$ (Oppenheimer & Davé 2006), plus the kinematics of damped Ly α absorbers (DLAs, Hong et al. 2009, in preparation). The mass loading factor (η , where $\dot{M}_{\text{wind}} = \eta \dot{M}_{\text{SF}}$) scales as σ^{-1} , meaning that lower mass galaxies are the most prolific enrichers by mass. This relation is central to reproducing the $z \sim 6$ galaxy luminosity function (Davé, Finlator, & Oppenheimer 2006), explaining the galaxy mass-metallicity relation (Finlator & Davé 2008), and providing a solution to the missing halo baryon problem (Davé 2009). The prescription even appears important for systems in the local Universe, as these wind simulations can account for the $z = 0$ missing metals (Davé & Oppenheimer 2007), the observed O VI forest at $z < 0.5$ (Oppenheimer & Davé 2009), and intragroup enrichment and entropy levels at $z = 0$ (Davé et al. 2008). While our simulations are only sensitive to the predicted wind scalings, and do not try to model the detailed physics of wind propagation, there is independent evidence that

other fundamental properties of galaxies are best understood by invoking momentum-driven winds (Hopkins et al. 2010).

One consequence of having highly mass-loaded, moderate-velocity outflows emanating from lower mass galaxies is that wind material remains in the relative proximity of their parent galaxies. Oppenheimer & Davé (2008, hereafter OD08) found that even when outflows launch in excess of a halo’s escape velocity, wind material regularly “recycles” back into a galaxy on a median timescale of 1-2 Gyrs. This occurs because winds are more slowed hydrodynamically by interactions with halo gas and gas outside halos rather than gravitationally. Winds typically reach ~ 100 physical kpc at all epochs, which means that outflows from $\geq M^*$ galaxies do not escape from their halo after $z \sim 1$. OD08 introduced the term *halo fountain* to describe such winds that remain trapped in their parent halos (see also Bertone et al. 2007). K09b coined *intergalactic fountain* to describe the transfer of feedback gas from low-mass galaxies at early times to higher mass galaxies at later times via a journey through the IGM.

A major implication of our wind models is that the amount of material ejected from galaxies is, globally over cosmic time, far larger than the amount of material forming into stars. Hence these outflow fountains recycling back into galaxies can in principle represent a significant reservoir for stellar mass formation over a Hubble timescale. This paper is devoted to examining such accretion, which we call “recycled wind accretion” (or just “wind mode”), in cosmological hydrodynamic simulations. In addition to hot and cold accretion, wind accretion effectively provides a third avenue for how galaxies get their gas. In this work we examine issues such as: How much of the cosmic stellar mass growth can this accretion mode create? Can this mode explain the preferred mass of galactic star formation at M^* (i.e. the knee in the Schechter function), as well as the faint-end slope of the GSMF? What happens to the GSMF if winds never recycle? Does wind mode need to be “quenched” at any particular mass, and if so what physics might produce this quenching?

In §2 we introduce our latest cosmological hydrodynamic simulations with several different prescriptions of superwind feedback. We begin to answer some of the above questions in §3 when we consider stellar mass growth divided into these component modes. We emphasise the concept of differential wind recycling as a function of galaxy mass and link it to the mass dependence of wind mode accretion. The effects of wind recycling on the GSMF are analysed in §3.4. Our purpose is not to precisely fit the $z = 0$ GSMF, but to introduce the concept of wind mode as a source of galaxy growth. We do argue that plausible wind models can come close to matching the observed GSMF, but only for galaxies below M^* . In §4 we discuss the balance of ejective and preventive feedback with recycled wind accretion. Ignoring wind mode, we examine how feedback suppresses star formation in §4.1, finding that no feedback implementation we explore can adequately explain the observed GSMF without wind mode. We then emphasise the effect of wind mode on the slope of the GSMF in §4.2. §4.3 examines whether wind mode is partly a numerical effect, especially above M^* where star formation-driven outflows are completely ineffective at quenching star formation. Finally, §5 summarises our findings.

2 SIMULATIONS

We employ the GADGET-2 N-body + Smoothed Particle Hydrodynamic (SPH) code (Springel 2005) to evolve a series of cosmological simulations to $z = 0$. We adopt a Λ CDM cosmology using cosmological parameters based on the 5-year WMAP results (Hinshaw et al. 2009): $\Omega_M = 0.28$, $\Omega_\Lambda = 0.72$, $h \equiv H_0/(100 \text{ km s}^{-1} \text{ Mpc}^{-1}) = 0.7$, a primordial power spectrum index $n = 0.96$, an amplitude of the mass fluctuations scaled to $\sigma_8 = 0.82$, and $\Omega_b = 0.046$. We refer to these simulations as the r-series, where our general naming convention for a simulation is r[boxsize]n[particles/side][wind model]. Our primary simulations use a boxsize of $48 h^{-1} \text{ Mpc}$ with 384 dark and SPH particles/side resulting in a dark matter particle mass of $1.8 \times 10^8 M_\odot$ and an SPH particle mass of $3.6 \times 10^7 M_\odot$. Gas particles on average spawn two star particles resulting in star particle masses averaging $1.8 \times 10^7 M_\odot$. We define the wind model suffixes at the end of this section.

An overview of the GADGET-2 code can be found in §2 of K09a. Additions to the public version of the code include cooling processes using the primordial abundances as described in Katz et al. (1996) and metal-line cooling as described in Oppenheimer & Davé (2006). Star formation is modelled using a subgrid recipe introduced in Springel & Hernquist (2003a) where a gas particle above a critical density is modelled as a fraction of cold clouds embedded in a warm ionised medium as in McKee & Ostriker (1977). The star formation follows a Schmidt law (Schmidt 1959) with the star formation timescale scaled to match the $z = 0$ Kennicutt law (Kennicutt 1998). The density threshold for star formation is $n_H = 0.13 \text{ cm}^{-3}$.

We use a Chabrier (2003) initial mass function (IMF) throughout, which has a turnover at masses $< 1 M_\odot$ relative to the Salpeter (1955) IMF. The fraction of mass in the IMF going into massive stars, defined here as $\geq 10 M_\odot$ and assumed to result in Type II supernovae (SNe), is $f_{\text{SN}} = 0.18$ in the Chabrier IMF. As our f_{SN} is larger than for the Salpeter IMF used in Springel & Hernquist (2003a, $f_{\text{SN}} = 0.10$), the amount of SN feedback energy coupled to the ISM is greater per unit star formation as is the energy input into galactic outflows in our standard constant-wind model (see below).

Our simulations directly account for metal enrichment from sources including Type II SNe, Type Ia SNe, and AGB stars. Gas particles eligible for star formation undergo self-enrichment from Type II supernovae (SNe) using the instantaneous recycling approximation, where mass, energy, and metallicity are assumed to immediately return to the ISM. Type II SN metal enrichment uses the metallicity-dependent yields calculated from the Chieffi & Limongi (2004) SNe models. Our prescriptions for feedback, described below, also assume the instantaneous input of energy from O and B stars (i.e. stars that are part of f_{SN}). We input the Type Ia SNe rates of Scannapieco & Bildsten (2005), where an instantaneous component is tied to the SFR, and a delayed component is proportional to the stellar mass as described in OD08. Each Type Ia SN adds 10^{51} ergs of thermal energy and the calculated metal yields of Thielemann et al. (1986) to surrounding gas, while the mass returned is comparatively negligible. AGB stellar enrichment occurs on delayed timescales from 30 Myrs to 14 Gyrs, using a star particle’s

age and metallicity to calculate mass loss rates and metallicity yields as described in OD08. AGB mass and metal loss is returned to the three nearest surrounding gas particles. OD08 showed that the largest effect of AGB stars is to replenish the ISM, because a star particle can lose nearly 40% of its mass over t_H , about double the $f_{SN} = 18\%$ that is recycled instantaneously via Type II SNe.

Feedback is directly tied to the SFR, using the relation $\dot{M}_{wind} = \eta \dot{M}_{SF}$, where η is the “mass loading factor.” The probabilities for an SPH particle with a non-zero SFR to turn into a star particle and to join a wind are calculated in each timestep; the ratio of the two probabilities is therefore η . Actual conversion into a star or wind particle is determined stochastically using these probabilities and a random number generator. We explore simulations with no winds and three different forms of implemented feedback.

No Winds (nw): No feedback energy is imparted kinetically to SPH particles. However, as with all simulations, energy is imparted thermally to ISM SPH particles using the Springel & Hernquist (2003a) subgrid two-phase recipe where all SN energy is instantaneously coupled to the ISM. The r48n384nw simulation can be compared to the GADGET-2 no wind simulation explored in K09a and K09b, although there are some notable differences. First, the cosmology is different; they use $\Omega_M = 0.26$, $\Omega_\Lambda = 0.74$, $h = 0.71$, $n = 1.0$, $\sigma_8 = 0.75$, and $\Omega_b = 0.044$. Second, the r-series uses a Chabrier IMF with delayed mass loss from AGB stars and feedback from Type Ia SNe, while the K09a simulation uses a Salpeter IMF and only Type II SNe feedback. The recycling of gas from AGB stars causes more late-time star formation in the r-series. A third difference is the addition of metal-line cooling for non-star forming SPH particles. This actually has little effect in the no wind case, because a vast majority of metals ($\geq 96\%$) remain within galaxies in either the ISM or star particles. We will find throughout §3 that the r48n384nw simulation reproduces the main mass growth properties (i.e. cold & hot mode) of the $50 h^{-1}$ Mpc, 2×288^3 particle simulation of K09a/b, although with some minor differences.

Constant Winds (cw): Feedback energy is added kinetically to gas particles at a constant rate relative to the SFR, with $\eta = 2$ and a constant velocity $v_{wind} = 680 \text{ km s}^{-1}$. This is intended to mimic the constant-wind model of Springel & Hernquist (2003a), however with some notable differences. Here η is defined relative to the SFR of the entire Chabrier IMF, and not just the long-lived stars in a Salpeter IMF as it is defined by Springel & Hernquist (2003a). Second, $v_{wind} = 680 \text{ km s}^{-1}$ is used rather than 484 km s^{-1} , because there is more SN energy per mass formed in a Chabrier IMF. The kinetic energy imparted to wind particles per unit star formation is $9.25 \times 10^{48} \text{ erg} / M_\odot$, which is 95% of the SN energy in this IMF assuming all stars $\geq 10 M_\odot$ add 10^{51} ergs/SN. Wind particles are hydrodynamically decoupled until either 2.9×10^7 yrs has passed or, more often, the SPH particle has reached 10% of the star formation critical density. Springel & Hernquist (2003b) demonstrated that this decoupling achieved resolution convergence. It is supposed to simulate the formation of hot chimneys extending out of a disk galaxy providing a low resistance avenue for SN feedback to escape into the IGM.

Slow Winds (sw): We simulate an alternative constant-wind model with the only difference being the

outflow velocities are half as high as the cw winds (i.e. $v_{wind} = 340 \text{ km s}^{-1}$ and $\eta = 2$). Therefore, only a quarter of the SN energy couples kinetically into these outflows.

Momentum-driven Winds (vzw): The momentum-driven wind model uses the scalings of Murray, Quatert, & Thompson (2005) based on the galaxy velocity dispersion (σ), and matches the observed trends of v_{wind} by Martin (2005a). Its implementation is explained in Oppenheimer & Davé (2006) and updated in OD08 with the addition of an in-run group finder to calculate σ using galaxy mass following Mo et al. (1998). One modification from OD08 is the in-run group finder now uses dark matter in addition to baryons to calculate masses as this produces better agreement across time with our post-run group finder (discussed below). The wind parameters vary across galaxies using the following relations:

$$v_{wind} = 3\sigma \sqrt{f_L - 1}, \quad (1)$$

$$\eta = \frac{\sigma_0}{\sigma}, \quad (2)$$

where f_L is the luminosity factor in units of the galactic Eddington luminosity (i.e. the critical luminosity necessary to expel gas from the galaxy potential), and σ_0 is the normalisation of the mass loading factor. Here we include a metallicity dependence additionally for f_L owing to more UV photons being output by lower metallicity stellar populations

$$f_L = f_{L,\odot} \times 10^{-0.0029 * (\log Z + 9)^{2.5} + 0.417694}, \quad (3)$$

randomly select $f_{L,\odot} = [1.05, 2]$ for each SPH particle, following observations by Rupke et al. (2005), and add an extra kick of size 2σ (the local escape velocity) to simulate continuous pumping of winds until it is far from the galaxy disk (as argued by Murray, Quatert, & Thompson (2005)). The only free parameter is $\sigma_0 = 150 \text{ km s}^{-1}$, which is the same efficiency factor of the mass loading used in OD08. Similar to the cw model, hydrodynamic forces are decoupled for a time of $1.95 \times 10^{10} \text{ km s}^{-1} / v_{wind} \text{ yr}$ or until 10% of the star formation critical density is reached; the latter is the case for the majority of wind particles.

The in-run group finder used to derive wind properties produces robustly consistent masses used to calculate σ compared to the post-run halo finder, although there are differences. The velocity dispersion of a halo, σ_h , scales as $M_h^{1/3}$, where M_h is derived by post-run. σ_h is different than σ calculated by the in-run group finder, which uses a higher threshold density to identify individual galaxies in groups and clusters rather than the dispersion of the entire group/cluster halo. Therefore, we find simulated winds have median values following $\eta \propto \sigma_h^{-0.95}$ between $M_h = 10^{10.7} - 10^{13.3} M_\odot$. The v_{wind} medians scale as $\sigma_h^{0.83}$, deviating from a linear relation owing primarily to lower metallicities from low-mass galaxies resulting in an extra boost (Equation 3); η does not depend on this equation. Because v_{wind} does not linearly scale with σ_h , winds launched from galaxies residing in groups and clusters are often launched below the halo escape velocity (v_{esc}); we explore this further in §3.2. At $z = 1$, a $10^{12} M_\odot$ halo identified by the post-run halo finder produces winds with median $v_{wind} = 490 \text{ km s}^{-1}$ and $\eta = 1.7$, equivalent to 40% of the total SN energy.

Our four simulations are listed in Table 1. They were run at the University of Arizona’s SGI cluster, ICE, the Na-

Table 1. Simulations^a

Name	v_{wind} (km s ⁻¹)	η^b	$E_{\text{wind}}/E_{\text{SN}}^c$
r48n384nw	–	–	–
r48n384cw	680	2	0.95
r48n384sw	340	2	0.24
r48n384vzw	$\propto \sigma$	$\propto \sigma^{-1}$	0.72

^a All simulations have 384³ SPH and dark matter particles in a 48 comoving h^{-1} Mpc box, corresponding to 1.8×10^8 and $3.6 \times 10^7 M_{\odot}$ per SPH and dark matter particle, respectively. They were all evolved to $z = 0$. The equivalent Plummer gravitational softening length is 2.5 comoving h^{-1} kpc.

^b η is defined as $\dot{M}_{\text{wind}} \propto \eta \times M_{\text{SF}}$.

^c Feedback energy divided by SN energy. Averaged over resolved galaxies for the r48n384vzw simulation.

tional Center for Supercomputing Applications’ Intel cluster, Abe, and the University of Massachusetts’ Opteron cluster, Eagle. Each simulation took between 100,000 and 150,000 CPU hours, although nearly 1 million CPU hours were used when including smaller box sizes and various test simulations.

We use the program SKID¹ to identify bound groups of cold baryons and stars (see K05 and K09a for more details). We have modified SKID with the requirement that bound gas particles must have non-zero SFRs; therefore we only identify gas in the galactic ISM and not from the extended halo. Our galaxy stellar mass limit is defined as ≥ 64 star particles, $M_s \sim 10^{9.05} M_{\odot}$, because Finlator et al. (2006) showed stellar properties of galaxies are well-converged above this limit. Halos are identified using a Spherical Overdensity algorithm with the same parameters as in K09a.

3 RESULTS

3.1 Modes of Star Formation

We begin our discussion of stellar mass growth by dividing gas accretion and star formation into its component modes. Just as in K05 & K09a/b, we divide hot and cold mode based on the maximum temperature, T_{max} , an SPH particle achieves on its journey into a galaxy. The temperature split is the same – $T = 2.5 \times 10^5$ K, which K05 justified as a good empirical division of the two modes. We define a third mode, *wind mode*, as any particle previously ejected in a wind that is re-accreted by a galaxy and forms stars (i.e. recycled). There is no temperature constraint on wind mode.

We have modified our version of GADGET-2 to track these three modes during a simulation using the following rules. An SPH particle’s T_{max} is tracked every timestep if it has not yet been launched in a wind. If the particle’s current temperature is greater than T_{max} , then T_{max} is set to the current temperature. T_{max} cannot be modified if a particle has a non-zero SFR, where the temperature is an average of the two-phase ISM model of Springel & Hernquist (2003a). Particle wind launches are also tracked, and T_{max} is not

allowed to be adjusted after such an event. Any star formation from a previously wind-launched particle is considered wind mode. For the purposes of this paper, we do not consider a particle’s T_{max} nor subsequent temperature history once it is launched in a wind. We also cannot properly track gas transferred via AGB feedback from star particles to surrounding gas particles, although this is a second-order effect that is not expected to favour any one mode; the transferred material will inherit the gas particle’s mode.

We consider the global star formation divided into these three modes for our four models in Figure 1. Our baseline for comparison is the no-wind (nw) simulation in the top panel. The black line is the global SFR density as a function of redshift, and the blue and red curves correspond to the hot and cold modes of star formation respectively; we use this colour scheme for these modes throughout this paper. The nw model is the focus of K09a and K09b, who use a lower resolution GADGET-2 simulation without winds as mentioned in §2. Our nw simulation shows the same qualitative characteristics identified by K09a including: (i) cold mode accretion dominates at all epochs, and (ii) the hot mode accretion fraction increases at late times; we refer the reader to their §3 for an in-depth discussion. However, note that Figure 1 plots star formation and not accretion (as was done in Figure 2 of K09a), although the two are tightly coupled (K05). Throughout this paper we consider only SFRs and not accretion rates, as our focus is on stellar mass growth; we leave a direct investigation of accretion rates for future work.

The next three panels of Figure 1 show the global SFR densities divided by mode for our three feedback models; the thin black line is the nw global SFR shown for comparison. In addition to the hot and cold modes indicated by the red and blue lines, the green lines in each of these panels indicate the contribution from the recycled wind mode. In every case, the wind mode dominates the global SFR over most of the history of the Universe. The wind mode contributes over 50% of the star formation after $z = 1.3, 2.7,$ and 1.7 for the cw, sw, and vzw models, respectively. The wind mode grows relative to the other modes at late times, making up 84%, 90%, and 92% of the $z = 0$ star formation, respectively. The resulting integrated stellar mass fractions in $z = 0$ galaxies are 51%, 73%, and 71%, respectively.

This leads us to our first main conclusion: wind material not only commonly recycles back into galaxies, it in fact *dominates* late-time stellar mass growth. Ejected material cannot be assumed to remain in the IGM forever. The wind mode and the total SFRs decline at late times, albeit at a slower rate than the cold and hot modes. SFRs are lower for every feedback simulation relative to the nw simulation, but the reduction is fairly minor for sw winds and vzw winds at later times. Outflows efficiently suppress both the cold and hot modes in all cases, but the wind mode re-supplies some of the ejected gas back into galaxies. Compared with the observed SFR density (Hopkins & Beacom 2006) (grey dashed lines), these two models over-predict star formation after $z > 1$, which we will argue in §4.3 is primarily a result of excessive star formation in $> M^*$ galaxies.

3.2 Differential Wind Recycling

Wind material recycles back into galaxies in a manner that depends on galaxy mass (OD08). This trend, which we re-

¹ <http://www-hpcc.astro.washington.edu/tools/skid.html>

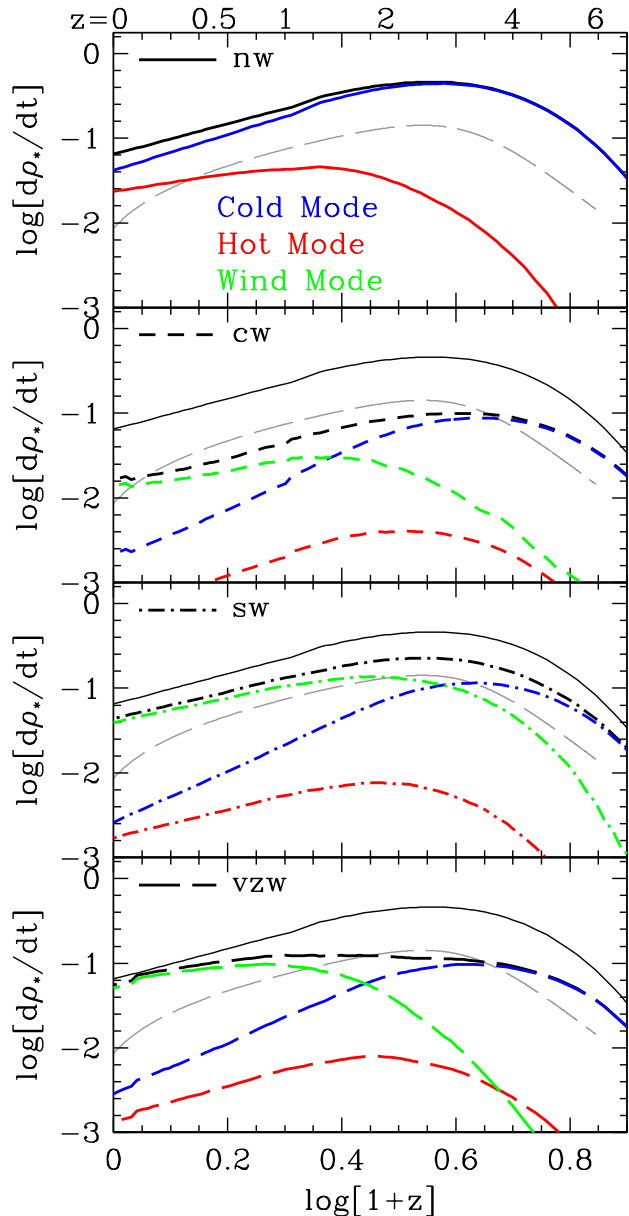


Figure 1. The global SFR density ($M_{\odot} \text{ yr}^{-1} \text{ Mpc}^{-3}$) in comoving units as indicated by the black lines, and sub-divided by accretion mode: cold (blue), hot (red), and wind (green). The integrated global no-wind SFR density is repeated with thin lines in the bottom three panels for comparison with each wind model. The grey dashed line indicates the Hopkins & Beacom. (2006) compilation calibrated to a Chabrier IMF. All galaxies (centrals and satellites) are included.

fer to as *differential recycling*, is key to understanding how recycling shapes the galaxy stellar mass function in these simulations. Wind recycling is defined as an event where a previously launched wind particle is either launched in a subsequent wind or converted completely into a star particle. The recycling time t_{rec} is defined as the time between the initial launch and re-launch/star particle conversion, which includes the time spent going out of the galaxy, the time spent coming back into the galaxy, and that spent within the new galaxy’s ISM. OD08 showed that individual wind particles average 2-3 wind launches (i.e. 1-2 recyclings) in

their vzw simulations with a median t_{rec} of $\lesssim 1$ Gyr, showing a weak dependence with redshift.

OD08 also showed recycling in the vzw model was highly dependent on a galaxy’s baryonic mass, with t_{rec} scaling as $\sim M_{\text{b}}^{-1/2}$ for vzw outflows. At face value this is surprising, since in this model winds are launched at speeds nearly proportional to v_{esc} of the galaxy. Hence if gravity were the dominant criterion for how far a wind travels and $v_{\text{wind}} < v_{\text{esc}}$, one should expect almost no trend with mass. By comparing the trends with analytic expectations, OD08 argued that hydrodynamical slowing dominates the wind deceleration, not gravitational forces. The deceleration is greater for more massive galaxies because they reside in denser gas environments, leading to quicker recycling. OD08 demonstrated that the gas outside halos is primarily responsible for hydrodynamic slowing in lower mass halos, while winds rarely escape the gas-rich halos of $> M^*$ galaxies at $z < 1$ (see their Figures 13 and 14).

Figure 2 plots t_{rec} as a function of the halo mass for central galaxies at the time they launch their winds. We focus on wind particles launched between $z = 1 \rightarrow 0.95$, for several reasons: (i) most wind mode accretion occurs below $z = 1$, (ii) there is ample time afterward (~ 8 Gyrs) to follow the outflow material, and (iii) there is a larger dynamic range in M_{h} to explore dependencies than at higher z . The curves at other redshifts do not differ dramatically from $z = 1$ for the same mass galaxy (see OD08). The black points correspond to individual wind particles; the vertical striping at higher halo masses results from the finite number of such halos. The un-recycled winds appear as the thin line of points at ~ 8 Gyrs. The lines show the times below which 10, 25, 50, 75, and 90% of launched particles recycle. If a line exists at a given M_{h} , then at least its corresponding fraction of particles recycle by $z = 0$ (e.g. if top dotted line exists, $\geq 90\%$ of winds recycle for that M_{h}). Finally, the histograms along the bottom show the relative number of integrated wind launches from all halos within a M_{h} bin. The statistics here only include central galaxies, which contain 87% of the total $z = 1$ star formation in each of the three models.

The purple curves show the analytical t_{rec} expected purely from gravity (i.e. freely falling trajectories) for each model. These are calculated by integrating the time-varying gravitational acceleration along a particle’s trajectory using the v_{wind} as the launch velocity and assuming Navarro, Frenk, & White (1997) halo potentials with concentrations from the Duffy et al. (2008) relation at $z = 1$ and a launch radius of $0.0125 r_{200}$. t_{rec} is twice the time needed to reach the turnaround radius, and is plotted if a particle is calculated to recycle before $z = 0$; no evolution for the halo is assumed. The median t_{rec} from the cw and sw models are shorter by $\times 2 - 3$ compared to the analytical case owing to hydrodynamic forces when $t_{\text{rec}} \gtrsim 1$ Gyr, confirming the argument of OD08 that hydrodynamic slowing plays a critical role in wind recycling. While winds in the vzw model are launched in excess of v_{esc} at high- z , this is not necessarily the case for galaxies $\gtrsim M^*$ at $z \lesssim 1$. Winds launched with $v_{\text{wind}} \propto \sigma$, where σ is calculated for an individual galaxy, cannot escape the group and cluster potentials in which such massive galaxies typically reside. We use the median v_{wind} tracked in the simulation for a given $z = 1$ M_{h} , therefore there exists some slight scatter from the expected $v_{\text{wind}} - M_{\text{h}}$ relation. This scatter becomes

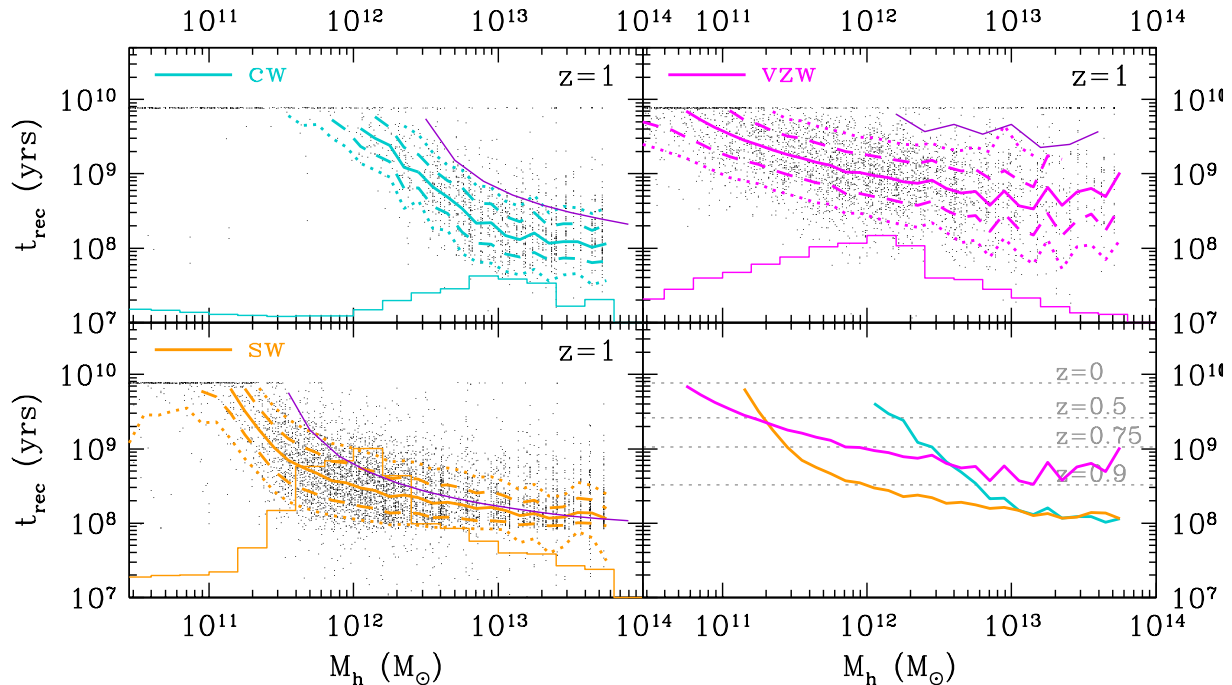


Figure 2. Recycling times – the time between when a wind particle is launched and when it is converted to a star or launched for a second time – for all wind particles ejected between $z = 1 - 0.95$ in the three wind simulations, as a function of the host galaxy’s M_h at launch time. Black dots show individual wind particles, and coloured solid lines show the median t_{rec} ; if this line exists for a given M_h then at least 50% of wind particles recycle. Similarly, 25 and 75% cuts on t_{rec} are indicated by dashed lines, while 10 and 90% cuts are indicated by dotted lines; if the top dotted line exists, $> 90\%$ of winds recycle. Purple lines show the expected t_{rec} from gravitational considerations alone. Histograms show the relative number of wind particles per M_h emanating from central galaxies. Wind events that escape until $z = 0$ contribute to the thin line of points at ~ 8 Gyrs, the time between $z = 1 \rightarrow 0$. The bottom right panel shows the diversity in the differential (i.e., mass-dependent) recycling curves (medians). Dotted grey lines, applicable for all models, indicate the redshift when median wind particles, launched at $\langle z \rangle = 0.975$, recycle.

amplified when performing the calculation of gravitational t_{rec} , leading to the non-monotonic trend of the purple line in the upper right panel. Gravitational forces play a significant role in slowing vzw winds, yet hydrodynamic slowing still reduces t_{rec} by $\times 3 - 5$.

The shape of the $t_{\text{rec}} - M_h$ relation for all the wind models we examined can generally be described by a power law decay of t_{rec} with mass followed by a gradual flattening. The differences between models can be seen explicitly in the bottom-right panel of Figure 2, where the median t_{rec} curves are compared. The cw model exhibits a steeper decline relative to the vzw model, which is simple to understand. The cw model has no dependence of outflow velocity on mass, leading to a greater gravitational deceleration at higher masses as the wind velocity falls below the typical v_{esc} of the halo. Another strong prediction of the cw model is, as expected, nearly no gas recycling occurs in halos with masses below $M_h \sim 3 \times 10^{11} M_\odot$. This is in sharp contrast to the vzw model where even low-mass halos experience significant rapid gas recycling. The sw model shows similar, but appropriately shifted, behaviour as the cw model, where the $t_{\text{rec}} - M_h$ relation has moved to lower mass corresponding to lower v_{esc} . Quantitatively, $t_{\text{rec}} \sim M_h^{-1.5}$ in cw versus $\sim M_h^{-0.6}$ in vzw over the range where t_{rec} reduces from 5 to 1 Gyr. Above $M_h \sim 10^{12} M_\odot$, the median t_{rec} in the vzw model flattens and never decreases much below 1 Gyr. This contrasts to OD08 where t_{rec} approaches 100 Myrs for the most massive galaxies. This difference owes to the fact that

we impose no speed limit in the simulations presented here whereas OD08 limits the E_{wind} to be no more than $2E_{\text{SN}}$, reducing the v_{wind} from massive galaxies.

Finally, the histograms of wind particle launches show significant differences between the models. These histograms are tied to the integrated SFRs per halo mass bin in central galaxies using the conversion factor η^{-1} . For the constant-wind models, this conversion factor is flat by definition, allowing the histogram to be a proxy indicator of the integrated star formation in central galaxies. The up-tick in the histogram at higher masses corresponds to the steep reduction in t_{rec} and is the signature of wind recycling significantly increasing star formation in higher mass halos at $z = 1$. This up-tick occurs at lower M_h in the sw model relative to the cw model, which we will show is related to the M_h where the wind mode dominates in the next subsection. Also, the integrals of each histogram are comparable between panels, and are proxies for the global $z = 1$ SFRs in Figure 1 (not including the minor contribution from satellites). The higher histogram of the sw model relative to the cw model results from the greater $z = 1$ wind mode SFRs. The vzw model cannot be so easily interpreted since η declines with halo mass.

To summarise, the wind velocity primarily sets the recycling time at a given halo mass, while the mass loading factor multiplied by the SFR determines the integrated amount of winds emanating from a given halo mass range (i.e. the histograms in Figure 2). The wind launch histograms increase

sharply where t_{rec} becomes small relative to t_{H} , which links differential recycling and the re-accretion of gas for star formation.

3.3 Star Formation and Stellar Masses

Having examined how winds recycle, we now consider this gas resupply as a source of star formation in Figure 3, where the SFR modes are decomposed as a function of M_{h} in our four models at three redshifts ($z = 3, 1, \text{ and } 0$). The data points represent individual galaxies, and the lines show the mean SFRs as a function of M_{h} . For the no-wind simulation in the top panels, we reproduce the main trends of K09a: (i) SFRs at a given redshift increase with halo mass, (ii) SFRs at a given M_{h} decline with cosmic time since at least $z = 4$, and (iii) cold mode star formation dominates at all redshifts and at almost every halo mass with the exception of intermediate masses at late times.

The lower three rows in Figure 3 correspond to our outflow simulations; all have wind mode SFRs that increase steeply with M_{h} (green lines), and which dominate above a certain M_{h} (except for the vzw model at $z = 3$). The key thing to note is that the wind mode begins to dominate at approximately the M_{h} where the median t_{rec} equals the Hubble time (cf. Figure 2 and $z = 1$ SFRs). Above this mass, wind recycling provides a gas supply that quickly exceeds the feedback-suppressed cold and hot modes.

Although outflows suppress the cold and hot modes in these simulations, it is the mass dependence of differential recycling that determines where and how much wind mode star formation occurs. For example, the cw SFR– M_{h} relations exhibit dramatic rises at $M_{\text{h}} \sim 10^{12} M_{\odot}$ at all redshifts, because the median t_{rec} falls below t_{H} above this mass. The sw SFRs increase steeply at $M_{\text{h}} \sim 10^{11} M_{\odot}$ for the same reason, resulting in the global SFR density becoming wind mode dominated at $z = 2.7$ compared to $z = 1.3$ for the cw (cf. Figure 1). In contrast, the vzw model does not show a preferred M_{h} where SFR dramatically increases, because the differential recycling curve is shallower and extends to lower masses. For the vzw model by $z = 0$, the wind mode dominates in halos above $2 \times 10^{11} M_{\odot}$, leading to more overall star formation in sub- M^* halos relative to the cw model.

The total SFRs of the wind models approach and even exceed the total no-wind SFRs (thin black lines) at higher masses at $z = 1$ and 0. In all our implementations, star formation-driven feedback appears unable to prevent star formation in massive halos. The sw SFRs are similar to the nw SFRs above $M_{\text{h}} = 10^{12} M_{\odot}$, at all redshifts. The sw winds, launched at 340 km s^{-1} , produce halo fountains with $t_{\text{rec}} \ll t_{\text{H}}$, which result in similar star formation rates as in the no-wind case. In some sense, this is similar to the canonical scenario for winds envisioned in e.g. Dekel & Silk (1986), where star formation-driven feedback has a strong impact on low mass galaxies but little impact at high masses, albeit for different reasons.

All the wind models show greater SFRs relative to the nw case in a range of halos by $z = 0$, with the sw and vzw SFRs exceeding the nw case for $M_{\text{h}} \gtrsim 10^{12} M_{\odot}$. In part, the enhanced late-time star formation reflects a delay, with wind ejection and recycling shifting star formation from early times to late times. In addition, wind recycling can shift star formation from low mass galaxies to high mass

galaxies via intergalactic fountains. Either way, wind recycling provides a greater reservoir of gas for late-time star formation. The resulting wind mode-dominated SFRs in high mass halos far exceed observed SFRs in the local Universe.

Figure 4 shows the cumulative contributions of cold, hot, and wind mode accretion to the $z = 0$ stellar mass of central galaxies. For the nw simulation, our results are similar to K09a/b: cold mode dominates at every mass, with a median contribution near 100% at low masses, 75% at $M_{\text{h}} \sim 3 \times 10^{11} M_{\odot}$, and 80-90% above $M_{\text{h}} \sim 5 \times 10^{12} M_{\odot}$. While direct cold mode accretion dominates at low masses, the highest mass galaxies are built largely from mergers of low-mass galaxies that formed *their* stars from cold mode gas (K09a). To reproduce the observed (much lower) masses of these galaxies, their low-mass progenitors must efficiently suppress star formation at early times, likely using an ejective feedback mechanism (K09b).

In contrast to the nw case, in all three wind models it is the wind mode that dominates the growth of high mass galaxies. The onset of wind mode dominance is swift in the cw and sw models, and slower in the vzw model owing to its shallower differential recycling curve. The transition mass where wind mode accounts for over half of the stellar mass growth occurs at $M_{\text{h}} = 10^{12.7}$, $10^{11.6}$, and $10^{11.4} M_{\odot}$ for the cw, sw, and vzw simulations respectively. The corresponding transition masses for the $z = 0$ SFR (right panels of Figure 3) are lower because recycled wind star formation occurs predominantly at late times. We show the link between M_{h} and M_{s} for central galaxies in Figure 4 using vertical grey lines drawn at the median M_{h} for central galaxies of $M_{\text{s}} = 10^9$, 10^{10} , 10^{11} , and $10^{12} M_{\odot}$. The grey lines move to higher halo masses for the 10^9 and $10^{10} M_{\odot}$ lines with the addition of feedback, because a galaxy with the same stellar mass will reside in a more massive halo owing to feedback suppression. The lines shift much less for $10^{12} M_{\odot}$ central galaxies as wind recycling renders feedback ineffective at limiting stellar mass growth for high-mass galaxies. In terms of stellar mass, wind mode accounts for over half of the stellar mass growth above $M_{\text{s}} = 10^{10.8}$, $10^{10.1}$, and $10^{9.8} M_{\odot}$ for the cw, sw, and vzw simulations respectively.

3.4 Galactic Stellar Mass Functions

We now consider stellar masses for *all* galaxies. Figure 5 shows the simulated $z = 0$ GSMFs including all accretion (thick lines) and excluding wind mode (thin lines). The latter case is equivalent to assuming wind materials never recycle and remain outside the ISM of any galaxy. Because SPH particles are tagged when first launched, all subsequent star formation can be removed from our analysis if particles recycle more than once. For comparison, we show the observed Bell et al. (2003) GSMF². As in K09b, the nw simulation significantly over-predicts the observed GSMF at all masses. The cw model changes from a nearly flat power law without wind mode ($\alpha = -2.11$ between $M_{\text{s}} = 10^{9.5} - 10^{10.5} M_{\odot}$) to having a bump above $M_{\text{s}} = 10^{11} M_{\odot}$ including all accretion. The result is a poor fit everywhere. Adding wind mode in the sw model flattens the GSMF the most between

² For alternative recent determinations of the GSMF, see Li & White (2009) and Bernardi et al. (2009).

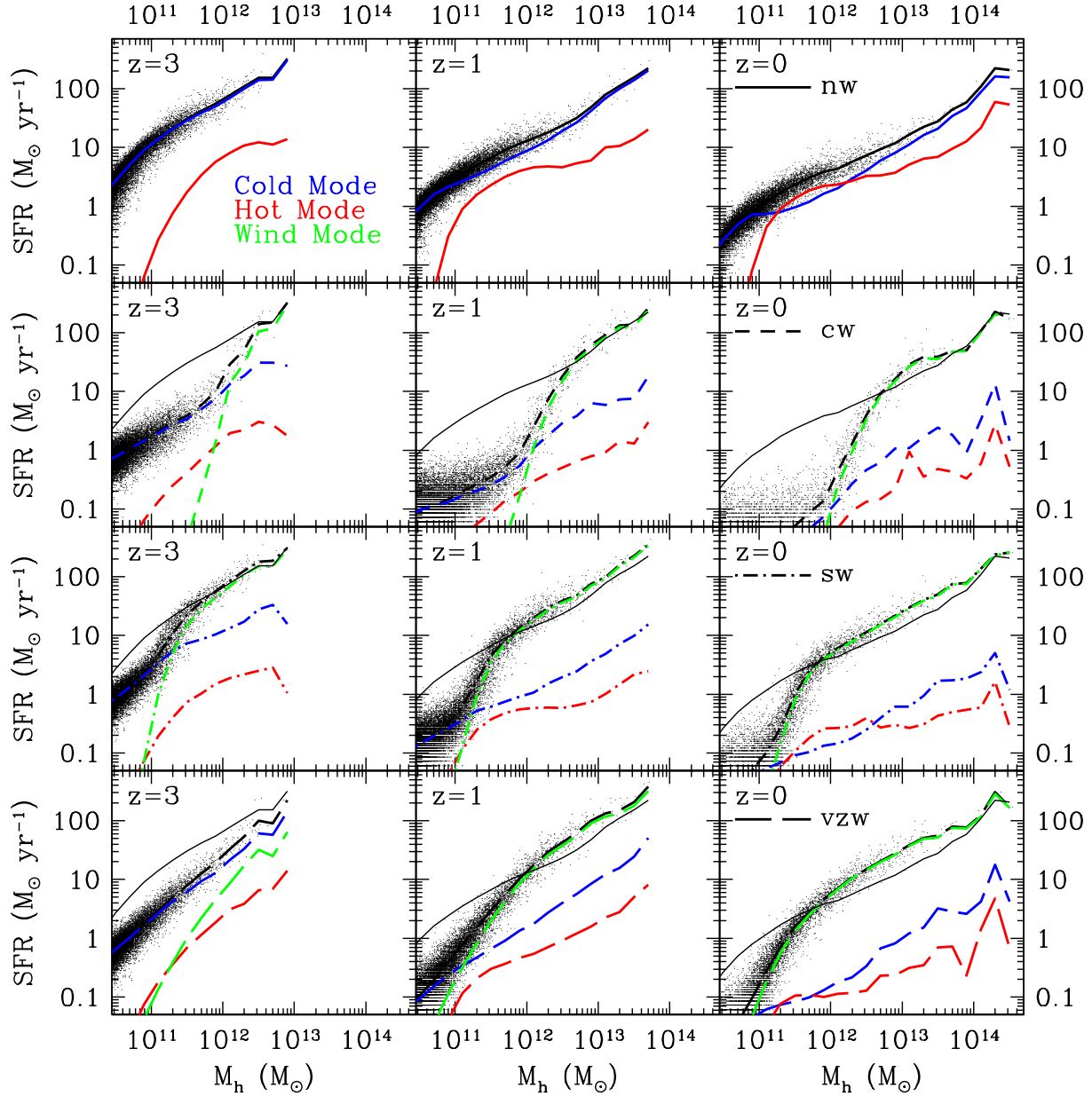


Figure 3. Instantaneous SFRs of central galaxies as a function of M_h for three redshifts ($z = 3, 1, 0$) in our four simulations. Black points show total SFRs of individual galaxies, and the black line shows the mean. Blue, red, and green lines show the mean SFR for cold, hot, and wind modes respectively. The thin black lines indicating the total nw SFR are repeated in the feedback model panels for comparison.

$M_s = 10^{9.9} - 10^{10.9} M_{\odot}$, from $\alpha = -2.18$ to -1.11 . The more gradual increase of wind mode with mass changes the vzw faint-end slope from $\alpha = -1.92$ to -1.45 over $M_s = 10^{9.5} - 10^{10.5} M_{\odot}$, and provides the best match to the observations at $M_s \leq 5 \times 10^{10} M_{\odot}$. Excluding wind mode yields acceptable agreement at the highest masses for the sw and vzw models, but it spoils the agreement at lower masses. We discuss the relative shapes of the various GSMFs further in §4.2.

To better characterise the impact of winds and wind recycling on galaxy masses, we rank order the galaxies in each simulation by stellar mass, then compare the properties of galaxies of the same rank in the different simulations.

In a statistical sense, this procedure picks out the directly comparable galaxies between pairs of simulations. Figure 6 plots the suppression factor, $f_{\text{supp}} = M_{\text{nw}}/M_{\text{wind}}$ relative to the stellar mass in the no-wind simulation, M_{nw} . A value $f_{\text{supp}} = 1$ (grey line in the figure) means that the rank-ordered masses between simulations with and without feedback are identical, i.e. feedback has had no effect. The solid black curve shows the value of f_{supp} required to obtain the mass of observed galaxies with the same comoving space density according to Bell et al. (2003); this is the quantity referred to as f_{corr} in K09b (their figure 1). The no-wind simulation produces galaxies that are too massive by a factor ~ 2.5 at $M_{\text{nw}} \sim 10^{11} M_{\odot}$, rising to a factor of 5–10 at the

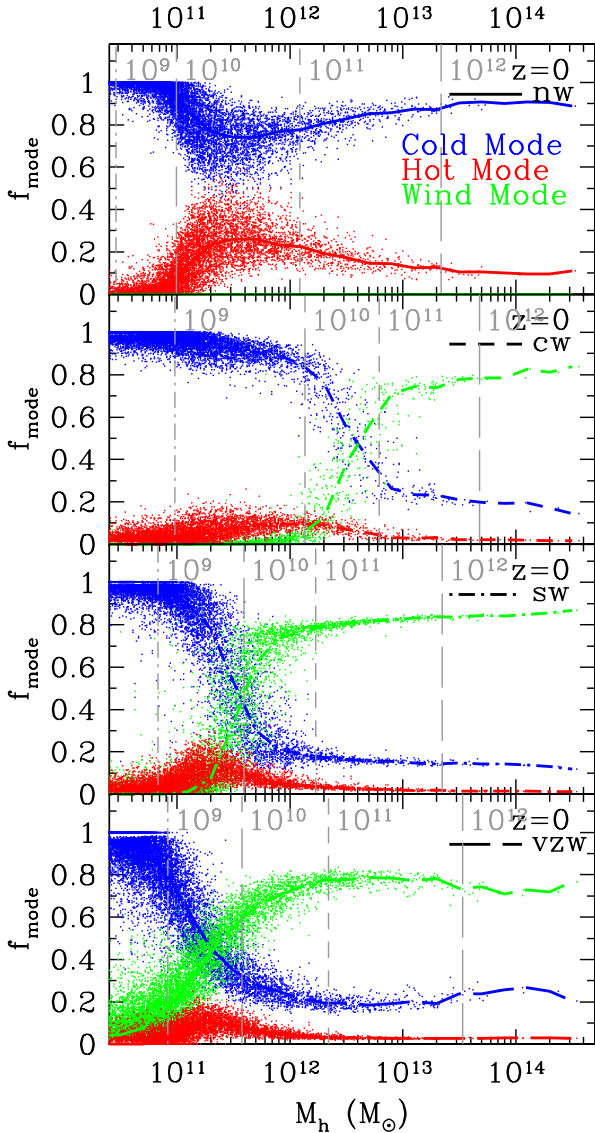


Figure 4. The fractional stellar mass of central galaxies assembled via the different modes as a function of halo mass. Coloured lines are medians of the fractional stellar mass growth corresponding to each mode. Cold mode dominates the no-wind simulation (top panel) at all halo masses, always exceeding 75% of the total mass growth. Cold mode exceeds hot mode in every feedback model (bottom three panels), but wind mode becomes the dominant growth mode at high M_h in every case. We indicate the relation between halo and stellar mass by grey vertical lines indicating the median M_h for the given M_s listed next to each grey line.

ends of the range plotted, similar to the findings of K09b. The vzw model traces this curve up to $M_{nw} \sim 7 \times 10^{10} M_\odot$, just as it agrees with the observed GSMF up to this mass scale in Figure 5. However, none of our models follows the black curve over the full mass range, just as no model reproduces the observed GSMF at all masses.

To compare the wind models to each other, we first consider the thin lines in Figure 6, which show f_{supp} when wind recycling is explicitly removed – i.e. any particle that was ever in a wind is not counted when computing the galaxies’ $z = 0$ masses. The mass suppression in the cw and sw mod-

els is considerably larger than the naively expected factor of $1 + \eta = 3$ (dotted grey line), for the reasons that will be discussed in §4.1 – the difference partly reflects the impact of mass recycling from evolved stars, but the dominant effect is that winds heat the surrounding gas and suppress accretion, providing preventive feedback in addition to ejective feedback. The suppression in these models is relatively independent of mass, compared to the steadily dropping f_{supp} in the vzw model owing to the $\eta \propto \sigma^{-1}$ scaling of the wind mass loading.

Including recycled wind mode (as our simulations do by default) changes the picture radically, as shown by the thick curves in Figure 6. For the cw and sw models, wind recycling has no impact on galaxies with masses below a threshold M_{nw} . For the slow winds of the sw model, f_{supp} approaches one above $M_{nw} \approx 10^{11} M_\odot$. The cw model shows a similar behaviour at an $\sim 8\times$ higher mass, but these faster winds suppress the masses of even the largest galaxies by a factor of two. The transition between the low and high mass regimes occurs at approximately the scale where $t_{rec} \approx t_H$ in Figure 2. f_{supp} in the vzw model also approaches one above $M_{nw} \approx 2 \times 10^{11} M_\odot$, but it continues to rise all the way to small masses unlike the constant wind models, which flatten towards the smallest masses.

The full f_{supp} curves show a much stronger mass dependence and much larger differences from model to model than the curves without wind mode. We conclude that it is the mass dependence of the recycled wind mode, what we have called differential recycling, that plays the strongest role in determining the shape of the GSMF in our simulations. In all the models, wind recycling leads to excessive stellar masses and star formation rates in massive galaxies compared to those observed. However, simply suppressing all wind recycling does not lead to an agreement with the observed GSMF. A model that resembled vzw, including recycling, up to $M_s \sim 10^{11} M_\odot$, but suppressed wind recycling with increasing effectiveness at higher masses would better match observations.

4 DISCUSSION

4.1 How Feedback Suppresses Star Formation

As noted in our discussion of Figure 6, in the absence of wind recycling, stellar mass suppression in the sw and cw models is considerably stronger than the naively expected factor of $1 + \eta = 3$. One may expect ejective feedback to reduce star formation by two thirds when $\eta = 2$, because two M_\odot of mass is ejected for every one M_\odot of stars formed. Part of the difference reflects the impact of stellar mass recycling (distinct from wind recycling). With our Chabrier IMF, 18% of the mass that forms stars is promptly recycled to the ISM as supernova and massive star ejecta, and over 10 Gyr this fraction rises to $\sim 50\%$, mostly from AGB winds. In a no-wind model, this recycled gas generally forms stars, increasing the galaxy stellar mass. However, in a constant-wind model, a fraction $\frac{\eta}{1+\eta}$ of the initial gas supply is ejected and hence never contributes any recycled stellar mass, and $\frac{\eta}{1+\eta}$ of the gas that is returned to the ISM by evolved stars is ejected rather than forming stars. With stellar recycling fractions of 50%, this effect alone can raise the mass suppression factor from 3 to ~ 5 .

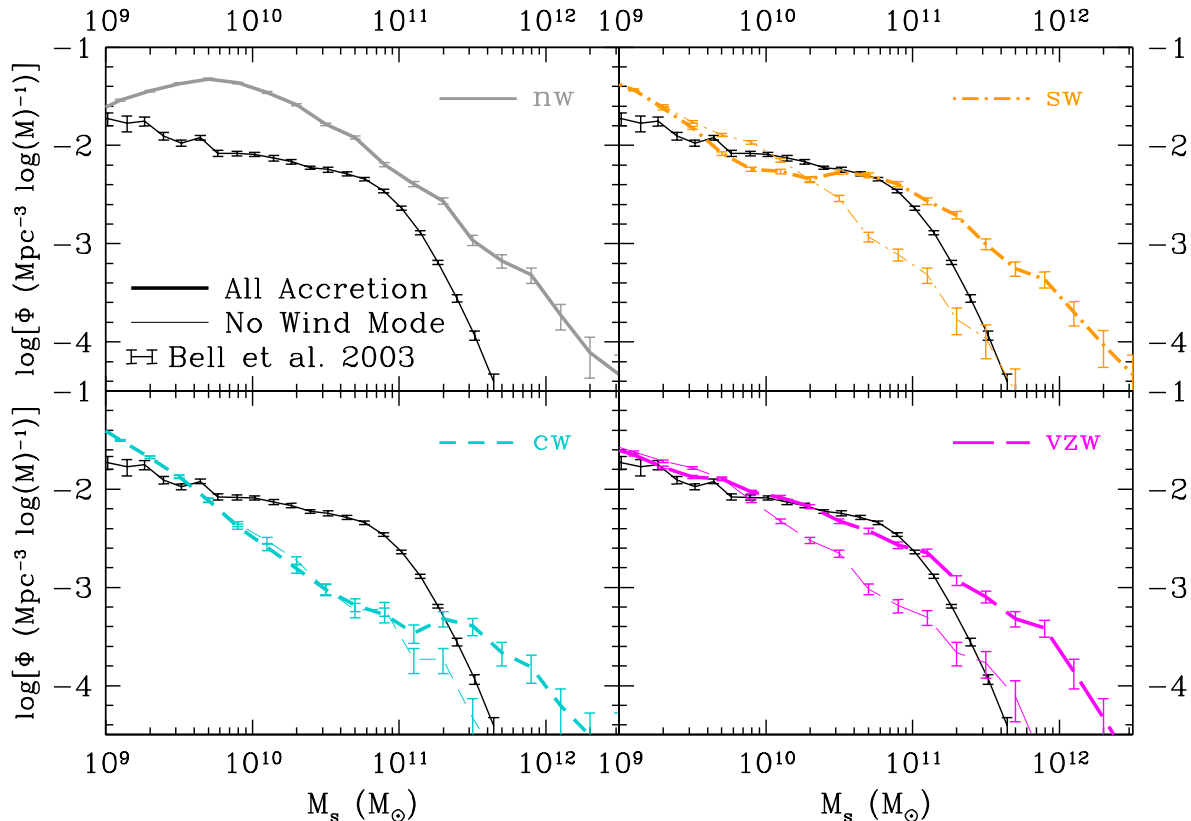


Figure 5. The $z = 0$ galactic stellar mass functions (GSMFs) for our four simulations including all accretion (thick lines) and without wind mode (thin lines); the no wind (upper left panel) simulation, by definition, has no wind mode. Also shown is the Bell et al. (2003) g -band derived GSMF (black) scaled to a Chabrier IMF for comparison.

Furthermore, winds inject energy and momentum into their surroundings and thereby suppress accretion, providing preventive feedback in addition to ejective feedback. This preventive feedback has the greatest impact on galaxies below M^* . To investigate this, we ran a cw simulation where we did not allow winds to interact hydrodynamically at all. The stellar masses *increased* by a factor in excess of 2 for the smallest galaxies we resolve. The energy added by these strong winds to the surrounding gas via hydrodynamic interactions is evidently playing a key role in suppressing gas accretion. This local “pre-heating” prevents IGM material from joining the filaments through which accretion is efficient. However, wind pre-heating is far weaker in the more moderate wind prescriptions. With only a quarter as much energy imparted to the surrounding gas, the sw winds result in galaxies twice as massive below $M_{\text{nw}} = 10^{11} M_{\odot}$ compared to the cw prescription (cf. the thin orange and cyan lines in Figure 6). The vzw winds have even lower wind energies at the low-mass end. Nevertheless, in all wind models cold mode SFRs decline faster at late times than expected from ejective suppression alone, likely owing to more dilute gas that can more easily be affected by energy input.

The vzw case also behaves somewhat differently than simple expectations. Outflow suppression does not rise as significantly as one would expect toward higher masses (thin magenta line in Figure 6), despite the $\eta \propto \sigma^{-1}$ scaling. If we assume $\sigma \propto M_b^{1/3}$, then $\eta \propto M_b^{-1/3}$ (at a given redshift), which OD08 showed is a fair description for the vzw mass

feedback rates. Over the range of $M_{\text{nw}} = 10^{10.3} - 10^{12.3} M_{\odot}$, we would expect an increase of f_{supp} by about a factor 4–5 in the vzw suppression efficiency relative to the constant mass loading of the cw and sw models given how η is calculated. However the increase appears to be at most a factor of 2, mainly because the more massive galaxies are the hierarchical merger products of low-mass progenitors, which had higher η before merging. This is the same argument K09a used to explain why massive galaxies are mainly assembled via cold mode – their progenitors are multiple small galaxies receiving gas via the cold mode channel. Thus, the higher η of the progenitors balance the low η of the merged galaxy at late times, reducing the differential mass loading effect.

These results show that, even in the absence of the recycled wind mode, the suppression of stellar masses does not follow simple scalings with the mass loading factor $\eta(M_b)$. Stellar mass recycling, hierarchical galaxy assembly, and, above all, the preventive feedback effects of winds (wind pre-heating), all act to complicate the mass dependence of feedback suppression. These results suggest caution when using analytic or semi-analytic models tied to the observed GSMF to infer the scaling of η with galaxy mass. Furthermore, we find that wind recycling changes the mass dependence of feedback suppression more strongly still, so model predictions will be sensitive to the assumptions (explicit or implicit) about the fate of gas after it has been ejected from the star-forming regions of its host galaxy.

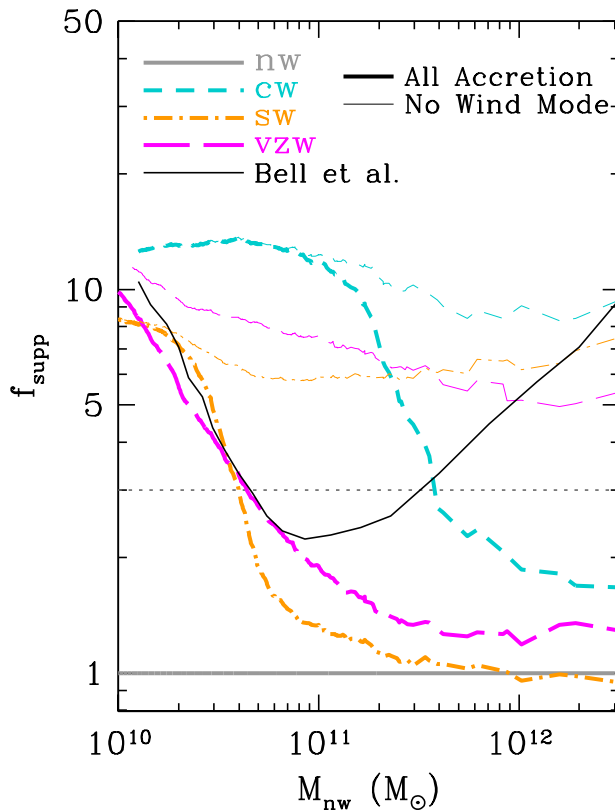


Figure 6. The suppression factor f_{supp} of galaxy stellar masses in feedback simulations relative to the stellar masses in the no-wind simulation. Galaxies are matched with the nw simulation by ranking them in order of decreasing stellar mass, then selecting galaxies of the same rank. Thick curves show results for the cw (cyan), sw (orange), and vzw (magenta) models. Thin curves show the results when recycled wind mode is explicitly removed. The black solid curve shows the required f_{supp} of no-wind stellar masses, M_{nw} , to match the masses of galaxies with the same comoving space density according from Bell et al. (2003). A model with f_{supp} following the black curve would reproduce the Bell et al. (2003) GSMF exactly. The dotted grey line shows the suppression naively expected from ejective feedback in the cw and sw wind models when recycling is suppressed.

4.2 Recycling and Faint-End Slopes of the GSMF

Differential recycling and wind mode creates much more diversity between the slopes of the mass functions (cf. thick coloured lines in Figure 5) than feedback suppression alone (thin lines). The sw model results in three distinct mass regimes, each with a different slope. At $M_s \lesssim 10^{10} M_\odot$ the slope remains steep until the wind mode significantly softens the slope as it increases sharply between $M_s \sim 10^{10} - 10^{11} M_\odot$. Above $M_s \gtrsim 10^{11} M_\odot$ the slope steepens again as efficient recycling causes it to approach the nw slope. This triple slope behaviour has also been identified in the Overwhelmingly Large Simulations (OWLS) when using a constant wind-type model (Marcel Haas, private communication, see also Crain et al. (2009)). The cw mass function could be described in a similar way, although with higher v_{wind} the “flattening” from the wind mode is better described as a bump at high masses. Increasing v_{wind} by a factor of two dramatically alters the $z = 0$ GSMF in two main ways: (i) preventive feedback suppresses by $\sim \times 2$

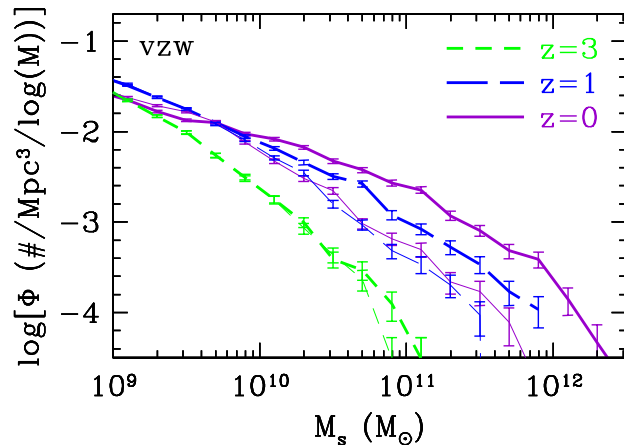


Figure 7. The GSMFs of the vzw model from $z = 3 \rightarrow 0$ including all accretion (thick lines) and without wind mode (thin lines).

cold and hot mode stellar growth at most masses, and (ii) wind mode galaxy growth begins at $\sim \times 8$ higher mass.

The vzw simulation manages to follow the faint-end slope of Bell et al. (2003) between $M_s = 10^9 - 10^{10.7} M_\odot$ fairly well. The flatter faint end is a direct result of the gradual differential recycled wind mode inherent in the vzw model. Above the threshold mass where recycling dominates, outflows behave as a series of fountains eventually becoming unable to escape their parent halo (i.e. the halo fountain phenomenon at $\gtrsim M^*$, OD08). Below the threshold mass where winds mainly escape into the IGM, wind mode contributes less to galaxies resulting in a very subtle steepening of the GSMF below $10^{9.5} M_\odot$, a milder version of the “triple-slope” behaviour in the sw model. Our resolution limit prevents us from concluding whether this simulated GSMF reproduces the “faint-end upturn” relative to a Schechter function, hinted at by the Bell et al. (2003) data and seen more clearly by Baldry et al. (2008); however we suggest the possibility this upturn could represent the transition mass below which wind mode stops contributing and the slope steepens.

Differential recycling also results in an evolution in the faint end of the GSMF, such that it is steeper at high redshifts when recycling is a small effect compared to direct accretion. Figure 7 demonstrates this evolution for the vzw model. Feedback sets the slope of the GSMF at all epochs; the steeper slopes at high- z ($z \gtrsim 2$) are set by the ejection of gas while the flatter slopes at late times are set by the recycling of gas. This evolution in the faint end has long been a challenge for hierarchical models, with only relatively ad hoc explanations proposed (see e.g. Khochfar et al. 2007). It is encouraging that our vzw wind model can fit the observed high- z GSMFs in Oppenheimer, Davé, & Finlator (2009, see also Davé, Finlator, & Oppenheimer 2006), while concurrently showing a number of other successes over other wind models in reproducing key galaxy and IGM statistics (see §1).

4.3 Is Wind Recycling a Numerical Artifact?

The detailed hydrodynamic and radiative interactions that might drive a galaxy’s ISM into outflows occur on scales

well below the resolution limit of any SPH simulations that model a representative cosmological volume. As discussed in §2, GADGET-2 uses a “sub-grid” model to store thermal energy from stellar feedback in the hot phase of a two-phase ISM, which slows star formation, pressurises and stabilises the ISM, and improves numerical convergence by lowering the sensitivity to mass resolution (Springel & Hernquist 2003a). However, this ISM pressure does not, on its own, lead to galactic-scale outflows, so GADGET-2, like some of its predecessors (e.g. Navarro et al. 1996), implements winds by imparting kinetic energy to individual particles (Springel & Hernquist 2003a). Winds are temporarily hydrodynamically decoupled as described in §2 to simulate the formation of hot chimneys extending out of a disk galaxy and to obtain resolution convergence in feedback simulations (Springel & Hernquist 2003b). Without this decoupling, it is still possible to drive winds that suppress star formation (Schaye et al. 2009) and enrich the IGM (Wiersma et al. 2009a), but the results do not remain well-converged with resolution (e.g. Dalla Vecchia & Schaye 2008). We have modified the GADGET-2 algorithm to implement the velocity scaling of momentum-driven winds (following OD08), but we have not altered the basic mechanism by which wind feedback is implemented. Our exploration of feedback in this paper is limited to kinetic feedback only, and other methods of feedback (e.g. SN blastwaves, Stinson et al. 2006) will result in different answers.

By construction, our scheme achieves its original goal, ejecting gas from star-forming galaxies with mass-loading factors and wind velocities that are motivated by a combination of theoretical and empirical arguments. Our results (and those of OD08) show that *re-accretion* of these ejected wind particles plays a major role in shaping the distribution of galaxy stellar masses and the correlations among halo mass, stellar mass, SFR, and redshift.

Unfortunately, there are a variety of numerical effects that could cause our modelling of the post-ejection behaviour of wind particles to be inaccurate. Most obviously, ejected wind particles initially have velocities and temperatures that are very different from those of their neighbours in the galaxy halo, while SPH is designed to represent fluid elements by groups of $N \geq 32$ particles. Second, SPH has known difficulties in treating two-phase media with sharp discontinuities in temperature and density, where gaps that develop around dense clumps tend to suppress instabilities that might otherwise break them apart (Agertz et al. 2007). Third, the ram pressure on under-resolved clumps (or single particles) can be overestimated because their smoothing lengths must be large enough to enclose 32 neighbours, which may give them an artificially large cross-section. K09a suggest that this excess ram pressure causes some or all of the “cold drizzle” of $T \approx 10^4$ K gas onto the central galaxies of massive halos (see also Naab et al. 2007). Fourth, our calculation of metal-line cooling is based on collisional equilibrium tables while Wiersma et al. (2009a) showed that photoionisation can significantly increase metal-line cooling times. In simulations without metal-line cooling, we find a significant decrease in wind recycling, and in overall gas accretion for galaxies above M^* , in general agreement with the findings of Choi & Nagamine (2009). Conversely, including the mixing of metals via instabilities, conduction, or diffusion (e.g. Wadsley et al 2008) would generally increase the

overall accretion in hot halos, as metal coolants spread over more mass decrease cooling times. Wiersma et al. (2009b) demonstrated that using smoothed SPH metallicities to simulate metal mixing can increase by 50% the number of baryons in stars compared to using single particle metallicities.

Wind recycling is unquestionably an important effect in our simulations, as we have shown in the preceding sections. It is a physically plausible phenomenon that doubtless occurs to some degree in the real Universe. However, given the numerical issues listed above, we cannot be sure that our simulations give an accurate quantitative account of the level of wind recycling that should arise in our adopted physical scenarios (cw, sw, and vzw). These numerical issues should be less severe for lower mass galaxies without hot halos, therefore the predictions for recycling relating to the sub- M^* galaxies and the GSMF faint-end slope should be more robust. It is worth reiterating that simulations with the GADGET-2 wind algorithm and the vzw scalings have achieved a number of empirical successes, including the $z = 6$ galaxy luminosity function (Davé, Finlator, & Oppenheimer 2006), the galaxy mass-metallicity relation (Finlator & Davé 2008), observations of IGM metal enrichment over a wide range of redshifts (Oppenheimer & Davé 2006, 2009; Oppenheimer, Davé, & Finlator 2009), and the shape of the $z = 0$ GSMF below M^* (this paper). These agreements do not depend much on the recycling behaviour in high-mass galaxies. Conversely, wind recycling contributes to the excessive masses and SFRs of super- M^* galaxies in high-mass halos, which is partially why the same simulations over-predict the global SFR density below $z \lesssim 1$ (Figure 1) and fail to reproduce the locally observed colour bimodality of galaxies (Gabor et al. 2010).

In comparing simulations with different mass resolutions (2×256^3 particles in 16, 32, and $64h^{-1}$ Mpc boxes), OD08 found similar qualitative results for wind recycling but significant changes in t_{rec} at a fixed galaxy mass. Further investigations of resolution and box size effects will be needed to characterise the numerical robustness of our quantitative results. In a different approach, we are using very high resolution simulations with idealised geometries to compare the behaviour of single-particle ejection to ejection of well resolved gas blobs (M. Peebles et al., in preparation). The strongest test of numerical robustness would be to carry out simulations that implement momentum-driven winds with a substantially different numerical algorithm; this is a longer term goal. At the same time, one can search for more targeted observational tests of our numerical predictions for galactic outflows and wind recycling, a point we return to below.

5 CONCLUSIONS

We have examined the factors that govern the present-day galaxy stellar mass function in cosmological hydrodynamic simulations that incorporate several different galactic outflow prescriptions. Our key result is the identification of a mode of accretion that we call recycled wind mode (or just wind mode), in which the accretion comes from material that was previously ejected from a galaxy.

This provides a third distinct accretion mode along with the “cold” and “hot” modes described by Kereš et al. (e.g. 2005); Dekel & Birnboim (e.g. 2006). At some level, the existence of a recycled wind mode is obvious – material ejected from galaxies can be subsequently re-accreted – but the impact on our simulations is remarkably large. In our simulation without winds, we recover the results of Kereš et al. (2009a/b), in which cold mode accretion dominates the growth of galaxy masses. In simulations with winds, however, wind recycling is the dominant mechanism of galaxy growth at $z \lesssim 1$.

Wind mode accretion occurs despite winds being ejected primarily at velocities exceeding the escape velocity of the galaxies’ halos. Hydrodynamic processes are mostly responsible for slowing the winds (as also argued by OD08). Even when the outflow speed is proportional to galaxy velocity dispersion, winds recycle back into more massive galaxies faster because they live in environments of higher gas density. The mass dependence of the wind mode we call *differential wind recycling*. In all three of our wind models, the median recycling time declines at higher halo masses, but the rate of decline depends on the wind prescription. In the most massive halos, the recycling time is typically below 1 Gyr, and $> 90\%$ of wind particles recycle without ever leaving their parent halos.

The differential wind recycling relations (§3.2) are mirrored in the galaxy SFRs decomposed by accretion mode (§3.3). Wind mode dominates the SFR of central galaxies approximately when t_{rec} becomes less than the Hubble time, so that the outflow material is then accreted back into galaxies at a rate exceeding the cold mode inflow. This transition to wind mode dominance is reflected in the stellar mass growth of $z = 0$ galaxies, as the galaxy stellar mass functions (GSMFs) from our three wind models show significant differences that are directly traceable to the behaviour of the wind mode in each case.

If we explicitly eliminate wind mode accretion in post-processing – by not counting recycled particles when computing galaxy stellar masses – then the $z = 0$ GSMFs of our three wind models are surprisingly similar to each other, and completely unlike the observed GSMF. The suppression relative to the no-wind simulation is much larger than the naively expected factor of $(1 + \eta)$, more so when high-velocity winds heat the surrounding gas and suppress subsequent accretion, providing preventive feedback in addition to the ejective feedback. When we include wind recycling (as our simulations do by default), then the GSMFs of the three wind models become quite different from one another, and the GSMF of the momentum-driven feedback (vzw) model agrees best with the Bell et al. (2003) data for galaxy stellar masses $10^9 M_{\odot} \leq M_s \leq 5 \times 10^{10} M_{\odot}$. The addition of wind mode flattens the faint-end mass slope from $\alpha = -1.92$ to -1.45 between $10^{9.5} M_{\odot} \leq M_s \leq 10^{10.5} M_{\odot}$. However, the predicted GSMFs greatly exceed the observed GSMF for $M_s \geq 10^{11} M_{\odot}$, approaching the prediction of the no-wind simulation, because material ejected in winds is quickly re-accreted in high mass halos.

Reproducing the observed $z = 0$ GSMF through wind mode alterations alone, at least in the vzw model, would require strong suppression of wind recycling at super- M^* masses ($M_h \gtrsim 2 \times 10^{12} M_{\odot}$), but minimal suppression of wind recycling at lower masses. It is conceivable that AGN

feedback could provide a mechanism for such mass dependent suppression, just as it has been invoked to suppress hot mode accretion in high mass halos (e.g., Croton et al. 2006; Cattaneo et al. 2009). However other mechanisms including virial shock heating (Birnboim et al. 2007; Naab et al. 2007) and gravitational heating by infalling satellites and cold gas clumps (Dekel & Birnboim 2008; Khochfar & Ostriker 2008) may suppress star formation without AGN, although the resolution in our cosmological-scale simulations may be insufficient to resolve such processes. Using semi-empirical modeling Hopkins et al. (2008) demonstrated that if star formation is efficiently quenched after major mergers of gas rich disks then the fraction of passive galaxies as a function of stellar mass is well matched to observations. Gabor et al. (2010) showed quenching mechanisms applied post-run to vzw simulations can produce a red sequence of galaxies without dramatically changing galaxies below L^* , although in detail none of the mechanisms tested there can exactly reproduce both observed luminosity functions and color-magnitude diagrams. Even if all star formation is quenched at M^* and above, this cannot account for the factor of $\sim \times 5$ greater SFR density than observed. Furthermore, Firmani et al. (2009) demonstrated recycling preferentially increases the specific SFR (SFR/M_s) in massive galaxies, which is in contradiction with observations showing the opposite trend. Simulations including self-consistent mechanisms to quench massive galaxy star formation may yield unexpected consequences for the star-forming sequence of galaxies.

We note that the impact of wind mode is particularly strong at late cosmic epochs, while at earlier times ($z \gtrsim 2$) the GSMF faint-end slope is set more by ejection. In our favoured wind model this causes the faint end to become shallower with time, which is qualitatively in agreement with observations. We leave a more detailed examination of such evolutionary trends for future work.

While wind recycling is an important effect in our simulations, we discussed (in §4.3) several reasons that our numerical treatment of winds and wind recycling could be inaccurate. Assessment of our predictions will require further testing of our sensitivity to numerical resolution, a study of the performance of the GADGET-2 wind implementation (particularly the single-particle ejection scheme), and consideration of alternative treatments of metal-line cooling. We can also look for direct observational tests of our numerical predictions of wind recycling and the distribution of ejected gas in galactic halos. One indirect line of evidence comes from the galaxy mass-metallicity relation (e.g. Tremonti et al. 2004), which implies a steep dependence of mass-loading factor on halo virial velocity, roughly $\eta \propto v_{\text{vir}}^{-3}$ (M. Peebles & F. Shankar, in preparation; R. Wechsler, private communication). This dependence, steeper than that expected for momentum- or energy-conserving winds, could potentially be explained by a combination of the σ^{-1} scaling for momentum-driven winds with the mass-dependent recycling rates that cause more massive galaxies to re-accrete much more of the enriched gas they once ejected. More direct tests of the simulation’s predictions can come from quasar absorption studies that probe metals and ionization states in the environments around galaxies. The advent of the *Cosmic Origins Spectrograph on Hubble Space Telescope* allows much more sensitive searches for low-redshift metals,

including tests of the Oppenheimer & Davé (2009) prediction that most metals traced by O VI reside near galaxies and frequently recycle.

Modellers have long argued that galactic outflows are a crucial element of galaxy formation, necessary to understand the shape of the galaxy luminosity function and the overall low efficiency with which cosmic baryons are converted into stars (e.g. White & Frenk 1991; Kauffmann et al. 1993; Cole et al. 1994; Somerville & Primack 1999)). Hydrodynamic simulations that explicitly incorporate winds into them are more successful than those without winds at reproducing other aspects of galaxy evolution and IGM enrichment. Those with moderate outflows from the majority of galaxies both effectively suppress star formation and enrich the nearby IGM where most metals are observed to reside (e.g. Stocke et al. 2006; Wakker & Savage 2009). Our results show that these outflows are by no means the end of the story – to understand how galaxies grow, one must understand, theoretically and observationally, the fate of the gas that they expel.

ACKNOWLEDGMENTS

We thank the referee, Avishai Dekel, for numerous suggestions that improved and clarified the paper. The authors also wish to thank Ari Maller, Kristian Finlator, Jared Gabor, Molly Peeples, Joop Schaye, Craig Booth, Marcel Haas, Ryan Quadri, Rob Wiersma, George Becker, and Richard Bower for encouraging discussion related to this research. The simulations run on the Intel 64 Linux Cluster Abe Supercluster at the National Center for Supercomputing Applications were greatly aided by the support staff there by providing us with dedicated nodes. We also thank the support staff for the ICE SGI cluster at the University of Arizona and Craig West at the Eagle Opteron cluster at the University of Massachusetts. Support for this work was provided by NASA through grant number HST-AR-10946 from the Space Telescope Science Institute. DW acknowledges the hospitality of the Institute for Advanced Study and the support of an AMIAS Membership.

REFERENCES

- Adelberger K. L., Shapley A. E., Steidel C. C., Pettini M., Erb D. K., & Reddy N. A. 2005, *ApJ*, 629, 636
- Agertz O., Moore B., Stadel J. et al. 2007, *MNRAS*, 380, 963
- Baldry, I. K., Glazebrook, K., & Driver, S. P. 2008, *MNRAS*, 388, 945
- Balogh, M. L., Pearce, F. R., Bower, R. G., & Kay, S. T. 2001, *MNRAS*, 326, 1228
- Bell, E. F., McIntosh, D. H., Katz, N., & Weinberg, M. D. 2003, *ApJS*, 149, 289
- Benson, A. J., Bower, R. G., Frenk, C. S., Lacey, C. G., Baugh, C. M., & Cole, S. 2003, *ApJ*, 599, 38
- Bernardi, M., Shankar, F., Hyde, J. B., Mei, S., Marulli, F., & Sheth, R. K. 2009, *arXiv:0910.1093*
- Bertone, S., De Lucia, G., & Thomas, P. A. 2007, *MNRAS*, 379, 1143
- Best, P. N., Kauffmann, G., Heckman, T. M., Brinchmann, J., Charlot, S., Ivezić, Ž., & White, S. D. M. 2005, *MNRAS*, 362, 25
- Birnboim, Y., & Dekel, A. 2003, *MNRAS*, 345, 349
- Birnboim, Y., Dekel, A., & Neistein, E. 2007, *MNRAS*, 380, 339
- Binney, J. 1977, *ApJ*, 215, 483
- Binney, J. 2004, *MNRAS*, 347, 1093
- Bower, R. G., Benson, A. J., Malbon, R., Helly, J. C., Frenk, C. S., Baugh, C. M., Cole, S., & Lacey, C. G. 2006, *MNRAS*, 370, 645
- Brooks, A. M., Governato, F., Quinn, T., Brook, C. B., & Wadsley, J. 2009, *ApJ*, 694, 396
- Cattaneo, A., et al. 2009, *Nature*, 460, 213
- Cen, R. & Ostriker, J. P. 2006, *ApJ*, 650, 560
- Chabrier G., 2003, *PASP*, 115, 763
- Chieffi, A. & Limongi, M. 2004, *ApJ*, 608, 405
- Choi, J.-H., & Nagamine, K. 2009, *MNRAS*, 393, 1595
- Cole, S., Aragon-Salamanca, A., Frenk, C. S., Navarro, J. F., & Zepf, S. E. 1994, *MNRAS*, 271, 781
- Crain, R. A., et al. 2009, *MNRAS*, 1262
- Croton, D. J., et al. 2006, *MNRAS*, 365, 11
- Dalla Vecchia, C. & Schaye, J. 2008, *MNRAS*, 387, 1431
- Davé, R., Finlator, K., & Oppenheimer, B. D. 2006, *MNRAS*, 370, 273
- Davé, R. & Oppenheimer, B. D. 2006, *MNRAS*, 374, 427
- Davé, R., Oppenheimer, B. D., & Sivanandam, S. 2008, *MNRAS*, 391, 110
- Davé, R. 2009, *arXiv:0901.3149*
- Dekel, A. & Silk, J. 1986, *ApJ*, 303, 39
- Dekel, A., & Birnboim, Y. 2006, *MNRAS*, 368, 2
- Dekel, A., & Birnboim, Y. 2008, *MNRAS*, 383, 119
- Dekel, A., et al. 2009, *Nature*, 457, 451
- Duffy, A. R., Schaye, J., Kay, S. T., & Dalla Vecchia, C. 2008, *MNRAS*, 390, L64
- Finlator, K., Davé, R., Papovich, C., & Hernquist, L. 2006, *ApJ*, 639, 672
- Finlator, K. & Davé, R. 2008, *MNRAS*, 385, 2181
- Firmani, C., Avila-Reese, V., & Rodríguez-Puebla, A. 2009, *arXiv:0909.5188*
- Gabor, J. M., Davé, R., Finlator, K., & Oppenheimer, B. D. 2010, *arXiv:1001.1734*
- Hinshaw, G., et al. 2009, *ApJS*, 180, 225
- Hong, S., Katz, N., & Davé, R. 2009, in preparation
- Hopkins, A. M. & Beacom, J. F. 2006, *ApJ*, 651, 142
- Hopkins, P. F., Hernquist, L., Cox, T. J., & Kereš, D. 2008, *ApJS*, 175, 356
- Hopkins, P. F., Murray, N., Quatert, E., Thompson, T. A. 2009, *MNRAS*, 401, L19
- Hutchings, R. M., & Thomas, P. A. 2000, *MNRAS*, 319, 721
- Jenkins, A., Frenk, C. S., White, S. D. M., Colberg, J. M., Cole, S., Evrard, A. E., Couchman, H. M. P., & Yoshida, N. 2001, *MNRAS*, 321, 372
- Katz, N., Weinberg, D. H., & Hernquist, L. 1996, *ApJS*, 105, 19
- Katz, N., Kereš, D., Davé, R., & Weinberg, D. H. 2003, *The IGM/Galaxy Connection. The Distribution of Baryons at z=0*, 281, 185
- Kauffmann, G., White, S. D. M., & Guiderdoni, B. 1993, *MNRAS*, 264, 201
- Kennicutt, R. C. 1998, *ApJ*, 498, 541

- Kereš, D., Katz, N., Weinberg, D. H., & Davé, R. 2005, MNRAS, 363, 2
- Kereš, D. 2007, Ph.D. Thesis
- Kereš, D., Katz, N., Fardal, M., Davé, R., & Weinberg, D. H. 2009, MNRAS, 395, 160
- Kereš, D., Katz, N., Fardal, M., Davé, R., & Weinberg, D. H. 2009, MNRAS, 396, 2332
- Khochfar, S., Silk, J., Windhorst, R. A., & Ryan, R. E., Jr. 2007, ApJ, 668, L115
- Khochfar, S., & Ostriker, J. P. 2008, ApJ, 680, 54
- Kobayashi, C. 2004, MNRAS, 347, 740
- Li, C., & White, S. D. M. 2009, MNRAS, 398, 2177
- Martin, C. L. 2005a, ApJ, 621, 227
- McKee, C. F. & Ostriker, J. P. 1977, ApJ, 218, 148
- Mo, H. J., Mau, S., & White, S. D. M. 1998, MNRAS, 295, 319
- Murali, C., Katz, N., Hernquist, L., Weinberg, D. H., & Davé, R. 2002, ApJ, 571, 1
- Murray, N., Quatert, E., & Thompson, T. A. 2005, ApJ, 618, 569
- Naab, T., Johansson, P. H., Ostriker, J. P., & Efstathiou, G. 2007, ApJ, 658, 710
- Navarro, J. F., Eke, V. R., & Frenk, C. S. 1996, MNRAS, 283, L72
- Navarro, J. F., Frenk, C. S., & White, S. D. M. 1997, ApJ, 490, 493
- Ocvirk, P., Pichon, C., & Teyssier, R. 2008, MNRAS, 390, 1326
- Oppenheimer, B. D. & Davé, R. A. 2006, MNRAS, 373, 1265
- Oppenheimer, B. D. & Davé, R. A. 2008, MNRAS, 387, 587
- Oppenheimer, B. D. & Davé, R. A. 2009, MNRAS, 395, 1875
- Oppenheimer, B. D., Davé, R., & Finlator, K. 2009, MNRAS, 396, 729
- Pettini M., Shapley A. E., Steidel C. C., Cuby J.-G., Dickinson M., Moorwood A. F. M., Adelberger K. L., & Galavisco M. 2001, ApJ, 554, 981
- Rees, M. J., & Ostriker, J. P. 1977, MNRAS, 179, 541
- Rupke, D. S., Veilleux, S., & Sanders, D. B. 2005, ApJS, 160, 115
- Salpeter E.E., 1955, ApJ, 121, 161
- Scannapieco, E. & Bildsten, L. 2005 ApJ, 629, L85
- Schaye, J., Aguirre, A., Kim, T.-S., Theuns, T., Rauch, M., & Sargent, W.L.W. 2003, ApJ, 596, 768
- Schaye, J., et al. 2009, MNRAS, 402, 1536
- Schechter, P. 1976, ApJ, 203, 297
- Schmidt, M. 1959, ApJ, 129, 243
- Shapley, A. E., Steidel, C. C., Pettini, M., & Adelberger, K. L. 2003, ApJ, 588, 65
- Sheth, R. K., & Tormen, G. 1999, MNRAS, 308, 119
- Silk, J. 1977, ApJ, 211, 638
- Simcoe, R. A., Sargent, W. L. W., & Rauch, M. 2004, ApJ, 606, 92
- Somerville, R. S., & Primack, J. R. 1999, MNRAS, 310, 1087
- Sommer-Larsen, J. & Fynbo, J. P. U. 2008, MNRAS, 385, 3
- Songaila, A., Cowie, L.L. 1996, AJ, 112, 335
- Songaila, A. 2001, ApJ, 561, L153
- Springel, V. & Hernquist, L. 2003, MNRAS, 339, 289
- Springel, V. & Hernquist, L. 2003, MNRAS, 339, 312
- Springel, V. 2005, MNRAS, 364, 1105
- Springel, V., et al. 2005, Nature, 435, 629
- Stinson, G., Seth, A., Katz, N., Wadsley, J., Governato, F., & Quinn, T. 2006, MNRAS, 373, 1074
- Stocke, J. T., Penton, S. V., Danforth, C. W., Shull, J. M., Tumlinson, J., & McLin, K. M. 2006, ApJ, 641, 217
- Thielemann, F.-K., Nomoto, K., & Yokoi, K. 1986, A&A, 158, 17
- Thoul, A. A., & Weinberg, D. H. 1995, ApJ, 442, 480
- Tremonti, C. A., et al. 2004, ApJ, 613, 898
- Wadsley, J. W., Veeravalli, G., & Couchman, H. M. P. 2008, MNRAS, 387, 427
- Wakker, B. P., & Savage, B. D. 2009, ApJS, 182, 378
- Weiner, B. J., et al. 2009, ApJ, 692, 187
- White, S. D. M., & Rees, M. J. 1978, MNRAS, 183, 341
- White, S. D. M., & Frenk, C. S. 1991, ApJ, 379, 52
- Wiersma, R. P. C., Schaye, J., & Smith, B. D. 2009, MNRAS, 393, 99
- Wiersma, R. P. C., Schaye, J., Theuns, T., Dalla Vecchia, C., & Tornatore, L. 2009, 399, 574